General Observations of the Time-Dependent Flow Field Around Flat Plates in Free Fall

Hærvig, Jakob; Jensen, Anna Lyhne; Pedersen, Marie Cecilie; Sørensen, Henrik

Published in:
Proceedings of the ASME/JSME/KSME 2015 Joint Fluids Engineering Conference

DOI (link to publication from Publisher):
10.1115/AJKFluids2015-12708

Publication date:
2015

Proceedings of of the ASME-JSME-KSME Joint Fluids Engineering Conference 2015
AJK2015-FED
July 26-31, 2015, Seoul, Korea

AJK2015-12708

GENERAL OBSERVATIONS OF THE TIME-DEPENDENT FLOW FIELD AROUND FLAT PLATES IN FREE FALL

Jakob Hærvig[*]
Department Energy Technology
Aalborg University
9220-Aalborg East, Denmark
Email: jah@et.aau.dk

Anna Lyhne Jensen
Department Energy Technology
Aalborg University
9220-Aalborg East, Denmark
Email: alj@et.aau.dk

Marie Cecilie Pedersen
Vattenfall Vindkraft A/S
Oldenborggade 25-31
7000-Frederica, Denmark
Email: mariececilie.pedersen@vattenfall.com

Henrik Sørensen
Department Energy Technology
Aalborg University
9220-Aalborg East, Denmark
Email: hs@et.aau.dk

ABSTRACT

The free fall trajectories of flat plates are investigated in order to improve understanding of the forces acting on falling blunt objects. The long term goal is to develop a general applicable model to predict free fall trajectories. Numerically the free fall of a flat plate is investigated using a six degrees of freedom (6DOF) solver and a dynamic mesh. To validate the simulation, the trajectories of aluminium plates falling in water are recorded by digital camera recordings and compared to the simulation. The simulation is able to calculate the motion of the plate within each time step with high accuracy, and thereby allowing the whole trajectory to be predicted with fair accuracy.

With the numerical model able to predict the free fall and the complex plate fluid interactions, fluids forces can be extracted for model development in future studies.

NOMENCLATURE

$\vec{A}$ Area vector pointing inwards
$\vec{F}_{\mathrm{g}}$ Gravity force
$\vec{F}_{\mathrm{r}}$ Resultant force
h Plate thickness
I^* Dimensionless moment of inertia
L Plate length
Re Reynolds number
$u_{\mathrm{t,a}}$ Terminal velocity
$\vec{u}$ Plate velocity
$\vec{v}$ Fluid velocity
p Static pressure
ρ Density
μ Dynamic viscosity
$\vec{\tau}_{\mathrm{w}}$ Wall shear stress

Subscripts
f Fluid
p Plate

INTRODUCTION

The unconfined motion of blunt objects falling in a viscous medium is a beautiful everyday example of time-dependent fluid dynamics. Examples include leaves or seeds falling from trees or playing cards being dropped. Documented interest in such phe-

[*]Address all correspondence to this author.

nomena date back to Maxwell who published a series of thoughts on what govern the falling motion of a slip of paper based on a series of simple experimental observations back in 1853 [1]. He furthermore noted that flat plates will fall with a two-dimensional trajectory if the third axis of the plate initially is held parallel to horizontal. Depending on the properties of the falling plate and the surrounding fluid, the plate will fall with different trajectories characterised by either steady falling motion, periodic oscillating motion, or tumbling motion. Examples of these regimes are given in Fig. 1. Until recently, investigations of these phenomena

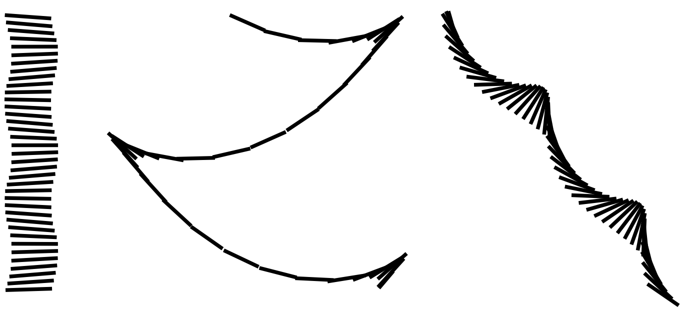

FIGURE 1. DIFFERENT TYPES OF FREE FALL TRAJECTORIES OBSERVED WHEN LETTING DIFFERENT PLATES FALL IN DIFFERENT FLUIDS: (A) STEADY FALLING REGIME; (B) PERIODIC OSCILLATING MOTION REGIME; (C) TUMBLING MOTION REGIME.

have only been carried out by experimental investigations. This includes Willmarth [2] and Field [3] who categorises the motion regimes for falling disks, and Smith [4] and Belmonte [5] who did a similar studies for falling flat plates. Common for these studies is the fact that they try to characterise the motion regimes in Fig. 1 based on the dimensionless Reynolds number and dimensionless moment of inertia:

$$\mathrm{Re} = \frac{u_{\mathrm{t,a}} L \rho_{\mathrm{f}}}{\mu} \tag{1}$$

$$I^* = \frac{8\rho_{\mathrm{p}} h \left(L^2 + h^2\right)}{3\pi\rho_{\mathrm{f}} L^3} \tag{2}$$

Furthermore, much research has been carried out by trying to describe the periodic oscillating motion regime including Tanabe [6], [7], Andersen [8], [9], and Pesavento [10]. Smith [4] mapped the different regimes in a Re$-I^*$ chart resulting in a substantial amount of data, which future models can be validated against.

Recent progress in Computational Fluid Dynamics and most of all computational power has allowed the time-dependent flow field around the falling plate to be investigated in details. These CFD simulations are expected to contribute with a better understanding of the different fluid forces which ultimately can results in a general model able to predict the trajectories. Therefore, the purpose of this study is to model the free fall trajectory of a flat plate in the periodically oscillaing regime by an experimentally validated CFD model.

Experimental Approach

The free fall will be investigated experimentally by recording the plate position and orientation as function of time. These trajectories are then compared to the one predicted by CFD.

Flat aluminium plates with density $\rho = 2700$ kg/m^3, length $L = 40$ mm, thickness $h = 2.0$ mm, and width $w = 206$ mm are dropped in a glass container with tap water at a well-defined inclination angle. The plates do not extend all the way to the glass container sides leaving 47 mm of free space on each side. As a result pressure driven tip vortices will be shed periodically around the ends of the plate, which can alter the trajectory. To minimise this effect the plate width is much higher than the plate length. The experiments by [4] and [9] used plate width to length aspect ratios of 3-4 and 15-30 respectively. In this study an aspect ratio of 5 is chosen, and no motion in the third dimension of significance is observed. Even though no motion in the third dimension is observed, the pressure distribution and therefore drag and lift are expected to deviate slightly from the purely two-dimensional case. To release the plates with well-defined initial conditions a vacuum pump is used as release mechanism. The instantaneous position and orientation are recorded by a digital Photon Focus MV1 camera with a Navitar 25mm f1.4 lens able to record a maximum of 170 frames per second at a resolution of 1300×1000 pixels. The experimental setup is sketched in Fig. 2. In this

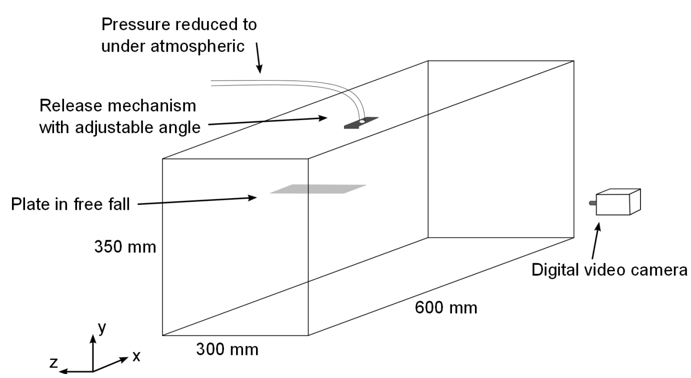

FIGURE 2. SKETCH OF EXPERIMENTAL SETUP USED TO RECORD THE FREE FALL TRAJECTORIES.

experiment a frame rate of 33.3 Hz was found sufficient to resolve both the instantaneous position and orientation while allowing enough light to be reflected from the plates. To remove extract the surroundings from the images and calculate the position and orientation of the plate in each image, the images are batch processed. For this purpose, a program in the LabVIEW Vision software suite was made. Figure 3 shows an example of a plate trajectory recorded by the procedure described in this section.

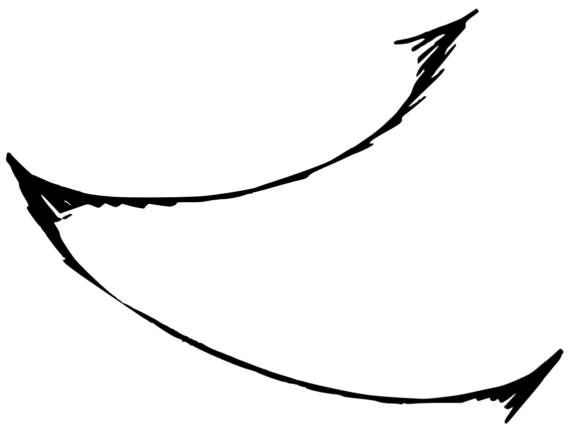

FIGURE 3. ALL INSTANTANEOUS FRAMES OF A FREE FALL SEQUENCE RECORDED BY THE EXPERIMENTAL PROCEDURE DESCRIBED ABOVE.

Numerical Approach

The simulations are set up using the commercial software ANSYS Fluent. The Reynolds-averaged Navier-Stokes equations are solved using the $k-\omega$ SST turbulence model [11]. A transient solver is used and a time step independence analysis suggested a time step size of 250 μs to make the results independent of the time step. A dynamic mesh is used to allow the plate to move between two successive time steps. To resolve the detailed flow phenomena around the plate, a structured mesh consisting of quadrilateral cells is placed around the plate. This part of the mesh follows the plate as it falls. Away from the plate, the dynamic mesh consisting of unstructured triangular cells is used. Fig. 4 gives an overview of the grid independent mesh following the plate as it falls. A rectangular computational domain being 20 plate lengths high and wide is used. A sketch of the domain is given in Fig. 5. To ensure reliable results, both grid, time, domain size independence analyses were carried out. To resolve the fine flow structures near the plate as it falls, 1.5 and 5 cells/mm along the plate length and thickness were required. Tab. 1 lists the results of the grid, time, and domain size independence analyses.

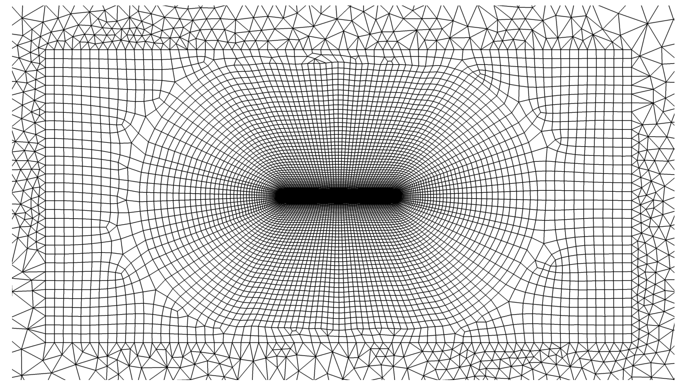

FIGURE 4. STATIONARY MESH CONSISTING OF QUADRILATERAL CELLS (FOLLOWING THE PLATE) AND AN UNSTRUCTURED MESH CONSISTING OF TRIANGULAR CELLS (DYNAMIC PART OF THE MESH).

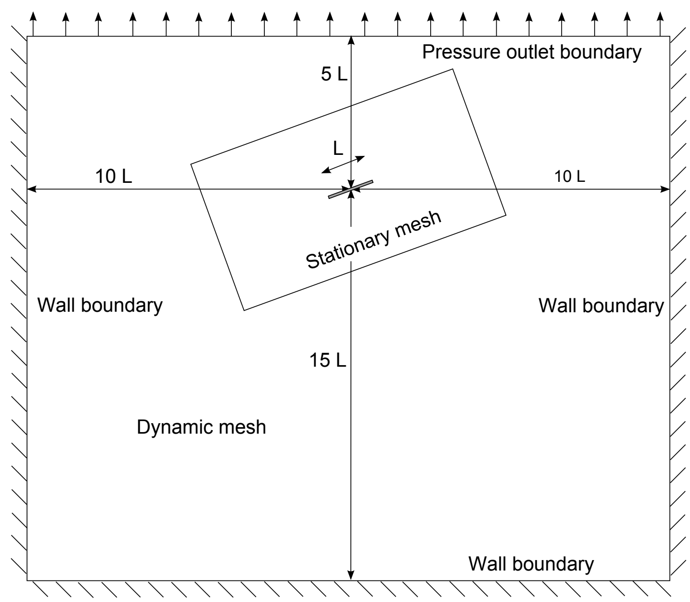

FIGURE 5. OVERVIEW OF THE COMPUTATIONAL DOMAIN USED FOR THE SIMULATIONS.

Dynamic Mesh

To track the motion of the plate, the commercially available 6 DOF solver in ANSYS Fluent is used [12]. For this simulation limited to two-dimensions, it reduces to a three degrees of freedom solver. This solver calculates the instantaneous fluid force $\vec{F}_r$

TABLE 1. RESULTS OF THE GRID, TIME, AND DOMAIN SIZE INDEPENDENCE ANALYSIS.

Parameter	Value
Total number of cells in domain	21,237 cells
Total number of quadrilateral cells	7,810 cells
Total number of triangular cells	17,488 cells
Cell density along plate length	1.5 cells/mm
Cell density along plate height	5 cells/mm
Domain size	$20\,L \times 20\,L$
Time step size	250 μs

on the plate by the sum of viscous, pressure, and gravity forces:

$$\vec{F}_{\mathrm{r}} = \int p \mathrm{d}\vec{A} + \int \vec{\tau}_{\mathrm{w}} \mathrm{d}A + \vec{F}_{\mathrm{g}}. \tag{3}$$

The instantaneous resulting fluid force is used to update the plate position and orientation between two successive time steps. The mesh is updated at every time step to ensure the criteria listed in Tab 2 are satisfied.

TABLE 2. CONFIGURATION OF THE DYNAMIC MESH USED FOR THE SIMULATIONS.

Parameter	Value
Minimum cell length	2.5 mm
Maximum cell length	1.7 mm
Maximum equiangular skewness	0.6

Results

A visualisation of the flow field in terms of velocity at different instances during a fall is presented in Fig. 6. By visualising the flow field, the fine flow details around the plate can be understood in details. At $t = 0.72$ s in Fig. 6a, the plate is aligned perfectly horizontally and the plate begins to elevate due to a high lift force, even though the angle of attack is close to zero. This lift force can be explained by the rotational motion of the plate resulting in an in-stationary boundary layer. In Fig. 6b, at $t = 0.82$ s the plate elevates with maximum vertical velocity. The deceleration of the plate, which started at around $t = 0.60$ s, has caused the surrounding fluid to continue past the plate resulting in a negative viscous force. The angle of attack begins to increase dramatically. At $t = 0.92$ s the plate reaches its extreme y-position. Due to the high orientation angle and zero x-velocity, the plate experiences the highest negative y- acceleration. The plate does however continue to rotate, resulting in a delay between the maximum x-position, y-position, and orientation angle. At $t = 0.97$ s the plate reaches its maximum orientation angle before it begins its long horizontal gliding motion. Fig. 7 shows a clear correspondence between the numerical result of plate trajectory and the mean trajectory from the experimental results. Small deviations are accumulated and the deviation is therefore increasing over time. It is seen that the turn of the plate occurs earlier in the CFD simulation than in the experiment. Fig. 8 and Fig. 9 compares the instantaneous accel-

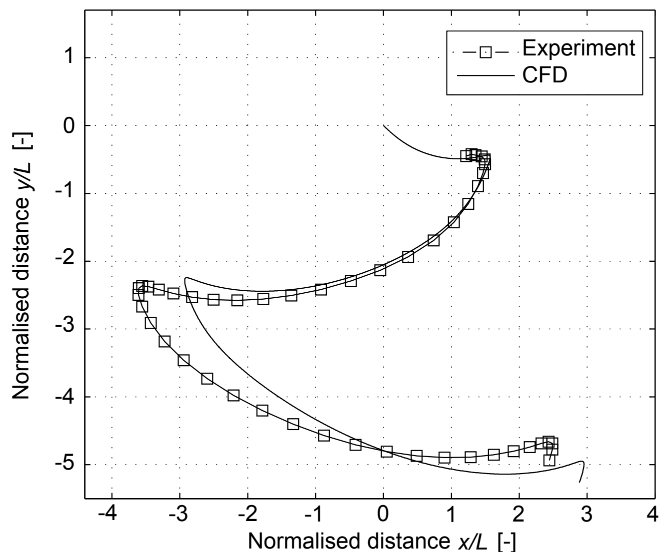

FIGURE 7. FREE FALL TRAJECTORY FROM EXPERIMENT AND CFD SIMULATION.

erations of the plate as a function of time from CFD and experiment in the x- and y-direction respectively. The instantaneous acceleration of the plate is interesting since it is directly linked to the instantaneous forces acting on the plate. The experimental result for acceleration is obtained by filtering the measured position as function of time and differentiating it twice. The two figures show great agreement between the experimental and the numerical results.

The arrows in Fig. 8 and Fig. 9 mark the instances visualised in Fig. 6. It is seen that the acceleration in the y-direction is accurately predicted at $t = 0.72$ s, where the plate translates at high velocity between two turns. Between $t = 0.82$ s and $t = 0.92$ s in Fig. 6(B) and Fig. 6(C) the y-acceleration in the experiment de-

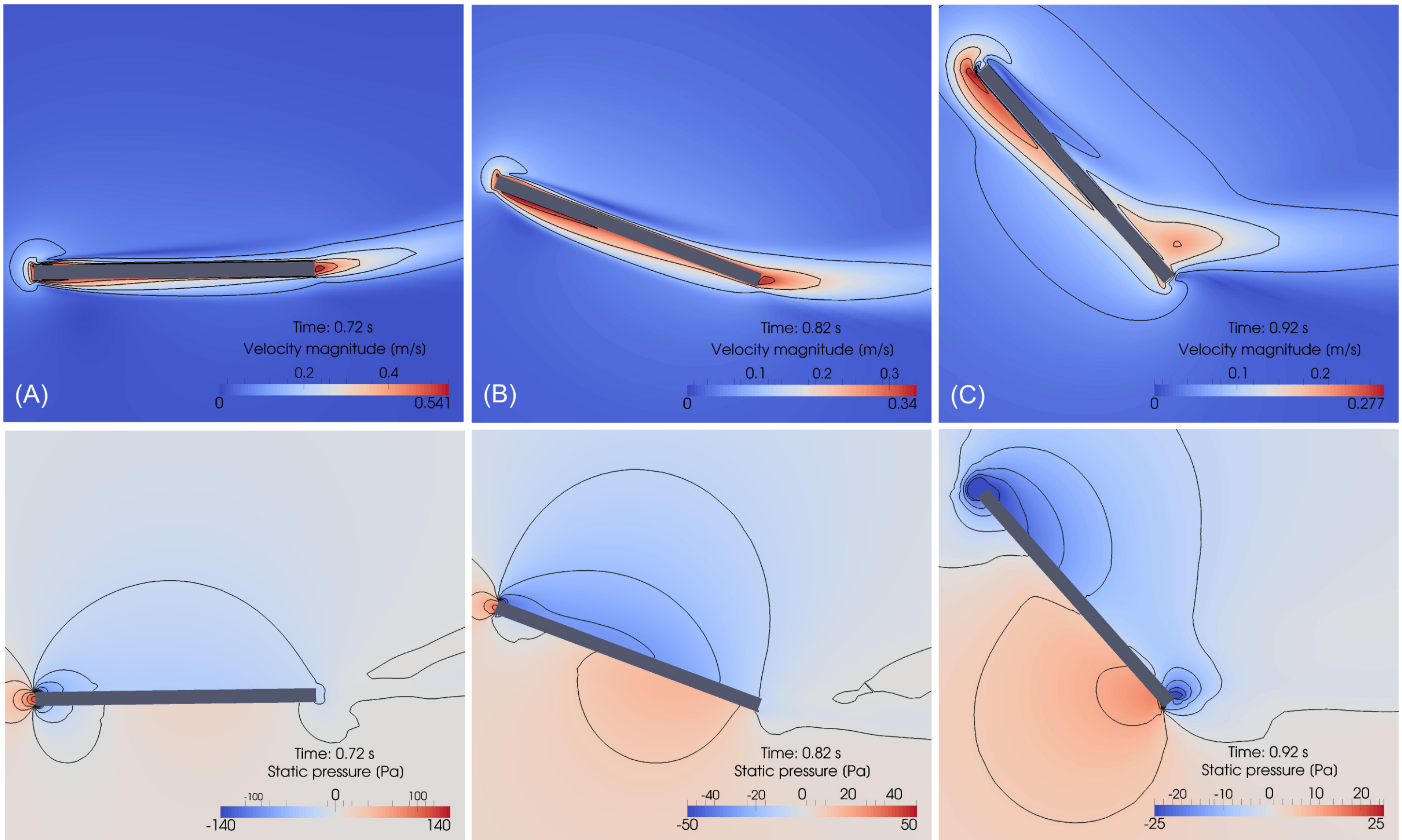

FIGURE 6. INSTANTANEOUS VELOCITY- AND PRESSURE FIELDS AROUND THE FALLING PLATE AT DIFFERENT INSTANCES: (A) THE PLATE IS PERFECTLY HORIZONTAL AND BEGINS TO ELEVATE DUE TO A HIGH LIFT FORCE; (B) THE PLATE ELEVATES WITH MAXIMUM VERTICAL VELOCITY WHILE THE FLUID CONTINUOUS PAST THE PLATE; (C) THE PLATE REACHES ITS EXTREME Y-POSITION. DUE TO A HIGH ORIENTATION ANGLE AND ZERO X-VELOCITY, THE PLATE ACCELERATE UPWARDS.

viates from the simulation and the negative y-acceleration in the simulation is larger than in the experiment. This is in agreement with Fig. 7 where the simulated plate moves upwards and turns earlier than the experimental result. This deviation might be due to 3D effects on the plate in spite of the quasi-two dimensional assumption.

The results deviate the most when the y-acceleration is high at approximately $t = 0.4$ s and $t = 0.9$ s corresponding to when the plate is turning. Along with the results presented in Fig. 7, this indicates that the assumption of the experiment being quasi two-dimensional is most uncertain in the turns.

Conclusion

A numerical model of a falling plate have been developed using a 6DOF solver and dynamic mesh, and validated by digital camera recordings of trajectories of aluminium plates in water. The validation revealed an overall very good agreement between numerical and experimental results. The largest deviations were present around the turning points in the trajectory. The deviations are expected to be due to 3D effects on the plate used in the experiments. The agreement between experiments and simulations are promising for the use of numerical data to better understand the forces on plates during a fall. The forces can be extracted from the numerical results and analysed with the aim of developing a generally applicable model able to predict plate trajectories.

REFERENCES

[1] Maxwell, J. C., 1853. “On a particular case of the descent of a heavy body in a resisting medium”. *Cambridge and Dublin Mathematical Journal,* ***9***, pp. 115–118.

[2] Willmarth, W. W., Hawk, N. E., and Harvey, R. L., 1964. “Steady and unsteady motions and wakes of freely falling disks”. *The Physics of Fluids,* ***7***, pp. 197–208.

[3] Field, S. B., Klaus, M., Moore, M. G., and Nori, F., 1997.

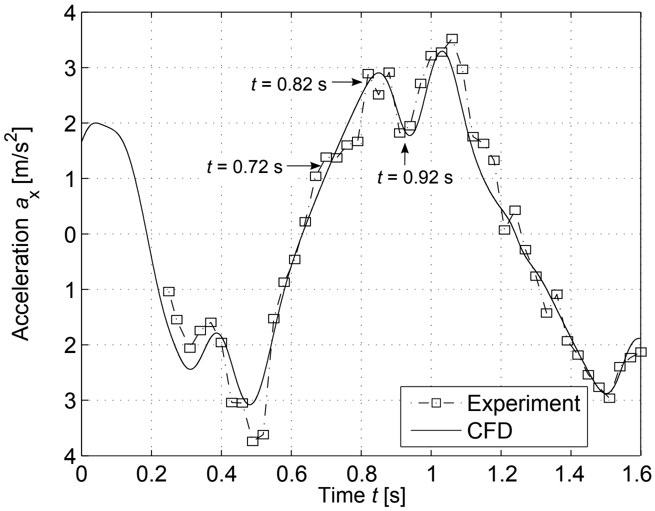

FIGURE 8. X-ACCELERATION AS FUNCTION OF TIME FOR THE CFD SIMULATION AND THE EXPERIMENT.

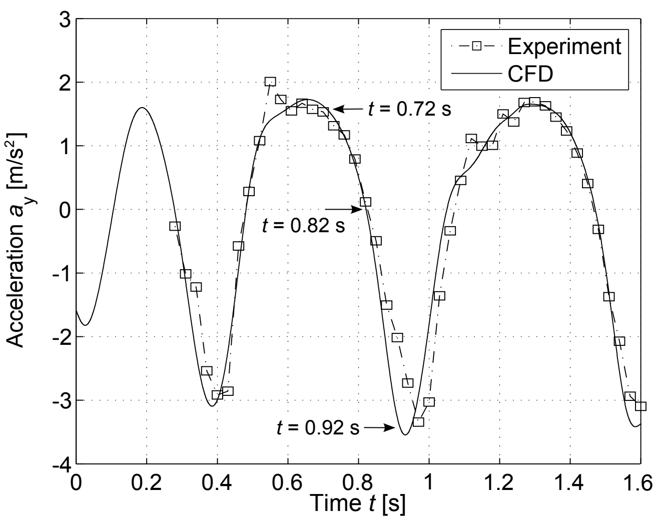

FIGURE 9. Y-ACCELERATION AS FUNCTION OF TIME FOR THE CFD SIMULATION AND THE EXPERIMENT.

"Chaotic dynamics of falling disks". *Nature,* ***388***, pp. 252–254.

[4] Smith, E. H., 1971. "Autorotating wings: an experimental investigation". *J. Fluid Mech,* ***50***, pp. 513–514.

[5] Belmonte, A., Eisenberg, H., and Moses, E., 1998. "From flutter to tumble: Inertial drag and froude similarity in falling paper". *Phys. Rev. Lett,* ***81***, pp. 345–348.

[6] Tanabe, Y., and Kaneko, K., 1994. "Behaviour of a falling paper". *Phys. Rev. Lett,* ***73***, pp. 1372–1377.

[7] Tanabe, Y., and Kaneko, K., 1995. "Comment on behaviour of a falling paper". *Phys. Rev. Lett,* ***75***, p. 1420.

[8] Andersen, A., Pesavento, U., and Wang, Z. J., 2005. "Analysis of transition between fluttering, tumbling and steady descent of falling cards". *J. Fluid Mech,* ***541***, pp. 91–104.

[9] Andersen, A., Pesavento, U., and Wang, Z. J., 2005. "Unsteady aerodynamics of fluttering and tumbling plates". *J. Fluid Mech,* ***541***, pp. 65–90.

[10] Pesavento, U., 2006. "Unsteady aerodynamics of falling plates". PhD thesis, Cornell University.

[11] Menter, F. R., 1994. "Two-equation eddy-viscosity turbulence models for engineering applications". *AIAA Journal,* ***32***, pp. 1598–1605.

[12] Snyder, D. O., Koutsavdis, E. K., and Anttonen, J. S. R., 2003. "Transonic store seperation using unstructured cfd with dynamic meshing". *AIAA 2003-3919,* ***33***.